ISSN 0915-633X

NATIONAL INSTITUTE FOR FUSION SCIENCE

Efficiencies of the ICRF Minority Heating in the CHS and LHD Plasmas

S. Murakami, M. Okamoto, N. Nakajima and T. Mutoh

(Received – Dec. 13, 1993)

NIFS-270

Jan. 1994

RESEARCH REPORT
NIFS Series

NAGOYA, JAPAN

Efficiencies of the ICRF Minority Heating in the CHS and LHD Plasmas

S. Murakami, M. Okamoto, N. Nakajima, and T. Mutoh

National Institute for Fusion Science,

Nagoya 464-01, Japan

Abstract

ICRF minority heatings are investigated in the plasmas of the Compact Helical System (CHS) and the Large Helical Device (LHD) by means of the orbit following Monte Carlo simulation. It is found that the heating efficiency decreases with increase of the absorption power by minority ions and depends strongly on the magnetic field strength and the field configuration.

Keywords: ICRF minority heating, the Compact Helical System, the Large Helical Device, heating efficiency, Monte Carlo simulation, magnetic field strength, field configuration

1. Introduction

Recent plasma heating experiments using the electromagnetic wave in the ion cyclotron range of frequencies[1-4] have been successfully carried out for non-axisymmetric systems and more high power ICRF heating experiments are planned for future devices[5]. However, because of the non-axisymmetric configuration, behaviors of high energy particles produced by the ICRF heating are so complicated that it is difficult to predict those behaviors and to evaluate the heating efficiency in a simple manner. In heliotron/torsatrons there are three typical behaviors of particle motions; the circulating particle, deeply trapped particle, and transition particle. Properties of these particles have been studied in detail[6-9]. However, it is difficult to predict the particle behaviors during the ICRF heating, because the particles interact with the ICRF wave and collide with the bulk plasma.

For the study of the ICRF minority heating in non-axisymmetric configurations we have developed the orbit following Monte Carlo simulation code[10]. This simulation method is also useful for studies of the neutral beam injection heating in non-axisymmetric configurations[11-15]. In our code, finite beta effects, complicated orbits of high energy particles, Coulomb collisions, and interaction between the particles and applied wave are included. In the previous paper we have studied the ICRF minority heating in the Large Helical Device (LHD)[5] and have shown the effects of finite plasma beta, radial electric field, and minority species on the heating efficiencies and the radial profile of transfer power to majority ions and electrons.

In this paper we study the ICRF minority heating for plasmas in the Compact Helical System (CHS) and LHD, and an emphasis is placed on the dependence of the heating efficiency on the magnetic field strength and the field configuration. In the followings we first explain the simulation model in Section 2. The results of Monte-Carlo simulation in the CHS plasma are shown in Section 3 and we here show the heating efficiency by changing the magnetic field strength and configuration. In Section 4 we show the simulation results in LHD plasma and compare with the results

of CHS case. Conclusions are given in Section 5.

2. Simulation model

Due to breaking of axisymmetry the angular momentum for the particle motion is not conserved and the particle orbits become complex depending on the field configuration in a helical system. Therefore, introduction of the realistic magnetic field configuration is necessary for evaluating the accurate particle orbits, losses, and resulting heating efficiency. To obtain the realistic magnetic field configuration precisely, we employ fully three dimensional MHD equilibria. The vacuum field is first calculated with real coil parameters and, then, we solve the three dimensional MHD equilibrium using the VMEC code[16]. The Boozer coordinates are introduced based on the obtained MHD equilibrium and we follow the particle orbits are in the Boozer coordinates taking into account Coulomb collisions with the bulk plasma and interactions with the ICRF wave.

By assuming the conservations of magnetic moment and the total energy, the motion of charged particle can be reduced to the four coupled ordinary differential equations in the Boozer coordinates[17]. By directly solving those four equations we obtain the motion of minority ions. The particle motions are followed until they escape from the plasma region. In this calculation we take the last closed magnetic surface as the boundary of particle losses.

The collisions of minority ions with majority ions and electrons are incorporated by introducing the collision operator developed by Boozer and Kuo-Petravic[18]. The linearized formula of collision operator for the energy and pitch angle scattering can be found based on the binominal distribution. We calculate the energy and pitch angle scattering by majority ions and electrons in every time step.

Minority ions are accelerated by RF electric field to heat majority ions and electrons through Coulomb collisions. Therefore temperatures of majority ions and electrons increase during applying ICRF heating. However, we fix the density and tem-

peratures of majority ions and electrons throughout the present calculations for simplicity. We will include the changes in the density and temperature of back ground species in the future calculations.

When a minority ion passes through the ion cyclotron resonance layer the particle interacts with the ICRF wave to change its velocity. In this calculation we assume the small parallel wave number, $kpl \sim 0$, and consider the velocity change due to the RF electric field only in the perpendicular direction and that is given by[19]

$$\Delta v_\perp = \frac{q}{2m} I\, e^{-in\phi_r} \left[|E_+|\ J_{n-1}(k_\perp \rho) + |E_-|\ J_{n+1}(k_\perp \rho)\right] \tag{1}$$

where ρ is the larmor radius, $\rho = mv_\perp/qB$, and J_n is the n-th Bessel function of the first kind. ϕ_r is the phase of the ICRF wave when the particle passes the resonance layer and we treat this value as a uniform random number between 0 to 2π. I is the function related to the resonance duration time. When the turning point dose not close to the resonance layer the duration time I is given by $I = \sqrt{2\pi/n\dot{\Omega}}$, where $\dot{\Omega}$ is the time derivative of the cyclotron frequency along the particle motion, $\dot{\Omega} = q/m(v \cdot \nabla)B$. As the turning point comes very near the resonance layer $\dot{\Omega}$ becomes zero ($v_{||} \simeq 0$) and the higher order correction in terms of $\ddot{\Omega}$ should be included. In this case I is given by[20,21] $2\pi\left(n\ddot{\Omega}/2\right)^{-1/3} Ai(0)$, where $Ai(0)$ is the value of Airy function $Ai(x)$ at $x = 0$. Finally the duration time I is given by

$$I = min\left[\sqrt{2\pi/n\dot{\Omega}},\ 2\pi\left(n\ddot{\Omega}/2\right)^{-1/3} Ai(0)\right]. \tag{2}$$

We consider only the fundamental resonance with the ICRF wave, $n = 1$, and assume $k_\perp \rho << 1$. The change in the perpendicular velocity is simply expressed as

$$\Delta v_\perp = \frac{q\,|E_+|}{2m} I\, e^{-i\phi_r}. \tag{3}$$

Using Eq. (3) we introduce the interaction of minority ions with the ICRF wave. We further assume that the applied wave electric field on the resonance layer, $|E_+|$, is spatially uniform over the resonance layer and fixed in time.

3. Efficiencies in the CHS plasma

We first show the results of the ICRF minority heating in the CHS plasma. The main parameters of CHS are shown in table I. Controlling the poloidal field, we can move the plasma horizontally to shift the magnetic axis position inward or outward. In the present calculations we consider two different configurations of CHS with the plasma beta at the center $\beta_0 = 0.0\%$; one is the configuration with the major radius position $R = 0.888$m and the other is $R = 0.921$m. In Fig. 1 the difference between the two magnetic configurations can be seen (in the Boozer coordinates). The plots of the mod-B_{min} contours that give the approximate orbit of deeply trapped particles[22] are shown for the two configurations in Fig. 1. From these figures we can see that the better confinement of deeply trapped particles can be obtained in the case of $R = 0.888$m (Fig. 1-(a)). For these two configurations we study the ICRF minority heating varying the absorbed power by the minority ions. We vary the absorption power by changing the amplitude of the ICRF wave, $|E_+|$, which is an input parameter for the calculations.

Initially all the minority ions are assumed to form a Maxwellian distribution in the velocity space;

$$f(v) = \frac{N}{(2\pi)^{3/2} v_{th}^3} \exp[-v^2/2v_{th}^2], \tag{4}$$

where N is the total number of minority ions used in the calculations and v_{th} is the thermal speed of initially loaded minority ions with a constant temperature of 150eV. Pitch angles of the minority ions are randomly distributed. The minority ions are initially loaded in the real space by

$$n(\overline{\psi}) = n_{m0} \exp[-c\overline{\psi}^2], \tag{5}$$

where $\overline{\psi}$ is the normalized toroidal flux function, $\overline{\psi} = \psi/\psi_a$ (ψ_a is the toroidal flux function on the last closed flux surface). Note that ψ is proportional to r^2, where r is the average minor radius. n_{m0} is the density of minority ions at the axis ($\psi = 0$) and c is the inverse of the standard deviation and set to be 4 in the present paper. The

particles are randomly distributed in the poloidal and toroidal directions.

The distributions of majority ions and electrons are given by

$$n_i(\overline{\psi}) = n_e(\overline{\psi}) = n_0(1-\overline{\psi})^{\alpha_1}, \quad (6)$$

$$T_e(\overline{\psi}) = T_{e0}(1-\overline{\psi})^{\alpha_2}, \quad (7)$$

$$T_i(\overline{\psi}) = T_{i0}(1-\overline{\psi})^{\alpha_3}, \quad (8)$$

where n_i and n_e are the density of majority ions and electrons, respectively, and T_i and T_e are the temperature of majority ions and electrons, respectively. We set the parameters as $n_0 = 3\times10^{19}\mathrm{m}^{-3}$, $T_{e0} = 150\mathrm{eV}$, $T_{i0} = 150\mathrm{eV}$, and $\alpha_1 = \alpha_2 = \alpha_3 = 1$. We assume the proton minority ion concentration is 10%. The ion cyclotron resonance layer can be controlled by changing the strength of resonance magnetic field and we set that strength to the value at the magnetic axis in the following calculation.

Figure 2 shows the plots of the power transferred from the minority ions to the bulk plasma, P_{trans}, as a function of the absorption power by minority ions, P_{abs}, in the case of $R = 0.888\mathrm{m}$. We change the strength of magnetic field; $B = 0.92\mathrm{T}$(closed circles), 1.4T(closed squares) and 2.0T(closed triangles). It is seen that the increasing rate of the transfer power becomes small as the absorption power rises and that this rate depends on the strength of magnetic field. In the case of $B = 0.92\mathrm{T}$ the lower increasing rate of P_{trans} is observed than that in the case of $B = 2.0\mathrm{T}$ when $P_{abs} > 200\mathrm{kW}$.

In order to evaluate the heating efficiency we introduce the power transfer rate, η, defined by P_{trans}/P_{abs} as a measure of the heating efficiency. Figures 3-(a) and (b) show the heating efficiency, η, as a function of P_{abs} in the two configurations. In both cases the decrease of the heating efficiency can be seen with increase of P_{abs} and higher efficiencies are obtained in the stronger magnetic field. This indicates that the heating efficiency strongly depend on the strength of magnetic field. Comparing the results of the two configuration cases it is found that the heating efficiency of $R = 0.888\mathrm{m}$ case is higher than that of $R = 0.921\mathrm{m}$ in all cases of magnetic field strength.

To clarify the dependence of the heating efficiency on the strength and configura-

tion of the magnetic field we consider a fitting function given by $\eta = 1/(1 + P_{abs}/P_0)$, where P_0 is an adjustable parameter and show the value of P_{abs} in which $\eta = 0.5$. By evaluating P_0 we discuss the dependence of the heat efficiency on the strength and configuration of the magnetic field. The plots of the fitting curves are shown in Fig. 3. We obtain the good agreement between the fitting curves and simulation results.

Figure 4 shows the values of P_0 in the two configurations as a function of the magnetic field strength in the two configurations; R = 0.888m (closed circles) and R = 0.921m (open circles). In all magnetic field strength cases of R = 0.888m the values of P_0 are about two times larger than those of R = 0.921m. The strong dependency of P_0 on the magnetic field strength can be seen. The relation $P_0 = \alpha B^\gamma$ can fit the calculated data if we chose α = 135.3 and γ = 1.28 in the case of R = 0.888m, and α = 67.8 and γ = 1.14 in the case of R = 0.921m. The larger value of α shows the better efficiency in the case of R = 0.888m and the value of $\gamma \sim 1.2$ shows the strong dependence of the heating efficiency on the magnetic field strength in both cases.

We here show the behavior of the minority ions to study the changes of particle orbits in the different strength and configuration of the magnetic field. Figure 5 shows the plots of typical orbits of minority ions during the ICRF heating in the two configuration and two magnetic field strength of CHS; (a) R = 0.888m and B = 2.0T, (b) R = 0.921m and B = 2.0T, and (c) R = 0.888m and B = 0.92T, where the initial velocities and positions are all the same. The magnetic surfaces of the initial particle position are shown by dotted lines.

Initially the particles are the circulating particle and move approximately along the magnetic field lines. During circulating the torus the particles pass through the resonance layer and the perpendicular energy of the particle increases. Then the particle becomes the trapped particle and can move across the magnetic surfaces.

Comparing the orbits of (a) and (b) we can see the difference between the particle orbits in the two configurations. In the case of R = 0.888m the particle is confined in the plasma region after the particle becomes the trapped particle. On the other hand,

the particle is lost after the change to trapped particle in the case of $R = 0.921\,\mathrm{m}$. This is because the confinement of the trapped particle is not good in the case of $R = 0.921\,\mathrm{m}$ (See Fig. 1-(b)).

The dependence of magnetic field strength on the particle orbit can be seen by comparing (a) and (c). In weaker magnetic field we obtain the larger ∇B drift velocity, $V_{\nabla B} \sim T/qlB$ (l is the characteristic length of magnetic field), and the finite banana orbit effect becomes large. Thus, the deviation from approximate orbit given by Fig. 1-(a) increases. In Fig 5-(a) and (c) the particle becomes the trapped particle at almost the same position. But the orbit of trapped particle reaches more outer region in the case of $B = 0.92\mathrm{T}$ and finally the particle is lost. That is due to the excursion caused by the larger drift velocity in the weak magnetic field.

Consequently, the strength and configuration of the magnetic field are important factors for the confinement of minority ions and, thus, the heating efficiency depends on the strength and configuration of the magnetic field.

4. Efficiencies in the LHD plasma

Next we show the results of ICRF minority heating in the LHD plasma. The main parameters of LHD are shown in table I. The magnetic configuration called "Standard configuration" of LHD[5] is considered in which the shift of the vacuum magnetic axis position, Δ, is –0.15m (0.15m inward shift) and the toroidally averaged magnetic surfaces are nearly circular in the vacuum field. This configuration satisfies the requirements for high plasma performance, i.e. good confinement of a single particle, high plasma beta value, and creating a divertor configuration. Using the VMEC code we also obtain the three dimensional MHD equilibrium based on the vacuum magnetic field with the coil parameters of the standard configuration. In this calculation we set the plasma beta at the center as $\beta_0 = 0.0\%$ in order to compare the results of the CHS with $\beta_0 = 0.0\%$. The dependence of the heat efficiency on the plasma beta has been discussed in the previous paper[10]. The temperature and density at the center

for majority ions and electrons are 1keV and $1\times10^{20}\mathrm{m}^{-3}$, respectively, and we assume the proton minority ions and 3% of minority ion fraction in the plasma. The strength of resonance magnetic field is set to the value at the magnetic axis.

Figure 6 shows the plots of the heating efficiency in the LHD plasma as a function of the absorption power, P_{abs}. We can see the similar decrease of the heating efficiency observed in the CHS case. However, the higher heating efficiency than that of CHS can be seen and the heating efficiency is higher than 0.6 even when $P_{abs} \sim 10$MW. In order to compare the dependence of heating efficiency on the configuration we also apply the fitting curve given by $\eta = 1/(1+P_{abs}/P_0)$ to the results of the LHD plasma. The solid line shows the fitting curve and the value of P_0 is 1.61×10^4kW. Using the relation $P_0 = \alpha B^\gamma$ and $\gamma \sim 1.2$ we can evaluate α as $\alpha = 4.3\times10^3$ and it is about 30 times better than that of the CHS plasma with $R = 0.888$m. Several reasons of this difference of α values between the CHS and LHD can be considered, e.g. device size, collision frequency, and particle confinement. Further studies are necessary for making clear the dependence of α value on those parameters.

5. Conclusions

We have studied the ICRF minority heating in the CHS and LHD plasmas using the orbit following Monte Carlo simulation code. The heating efficiencies as a function of the absorption power by minority ions have been shown with changing the strength and configuration of the magnetic field. As the absorption power by minority ions rises the heating efficiency decreases due to the increase of power loss by the particle orbit loss. We have found that the heating efficiencies strongly depend on the magnetic field strength and the field configuration. This is confirmed by comparing the orbit of minority ions with different strength and configuration of the magnetic field.

Our results in the CHS suggest that the more strong magnetic field strength and the better configuration for particle confinement are necessary for the efficient ICRF minority heating. And comparison of results in the CHS and LHD shows the remark-

able advantage of ICRF minority heating in the LHD.

However, in the CHS the improvement of the heating efficiency can be possible by changing the following conditions. In our calculations we have used protons as a minority species and the higher heating efficiency is obtained by applying the ^{3}He minority ions[10] because of the increase of Coulomb collisions with the bulk plasma and the decrease of orbit loss. By increasing the minority ion concentration we can also improve the heating efficiency due to the reduction of the averaged energy of minority ions and the two-ion hybrid mode conversion process where direct electron heating occurs. In the CHS plasma the competition of the minority heating and the mode conversion process is possible in the ICRF heating and would improve the heating efficiency largely.

Acknowledgements

The authors wish to thank Dr. K. Nishimura, Dr. K. Y. Watanabe, and Dr. M. Ohnishi for useful discussions. Members of ICRF heating Group and CHS Group at the National Institute for Fusion science are also acknowledged. They thank Prof. A. Iiyoshi and Prof. T. Sato for continuous encouragement. The calculations were carried out on the super computer SX-3 at the National Institute for Fusion Science.

References

[1] T. Mutoh, et al., Nucl. Fusion **24** (1984) 1003.

[2] T. Mutoh, et al., in Plasma Physics Controlled Nuclear Fusion Research 1986 (Proc. 11th Int. Conf. Kyoto, 1986), Vol. 2, IAEA, Vienna (1987) 473.

[3] M. Kwon, et al., Nucl. Fusion **32** (1992) 1225.

[4] V. V. Bakaev, et al., in Plasma Physics Controlled Nuclear Fusion Research 1984 (Proc. 10th Int. Conf. London, 1984), Vol. 2, IAEA, Vienna (1985) 397.

[5] A. Iiyoshi, et al., Fusion Technol. **17** (1990) 148.

[6] H. E. Mynick, H.E., Phys. Fluids **26** (1983) 1008.

[7] K. Itoh, et al., Nucl. Fusion **29** (1989) 1851.

[8] K. Itoh, et al., Phys. Fluids B **3** (1991) 1294.

[9] J. Todoroki, J. Phys. Soc. Jpn. **59** (1990) 2758.

[10] S. Murakami, et al, (submitted to Nucl. Fusion)

[11] K. Hanatani, et al., Nucl. Fusion **21** (1981) 1067.

[12] K. Hanatani, F. -P. Penningsfeld, Nucl. Fusion **32** (1992) 1769.

[13] R. N. Morris, et al., Fusion Technol. **12** (1987) 281.

[14] R. H. Fowler, et al., Fusion Technol. **20** (1991) 200.

[15] R. H. Fowler, et al., Nucl. Fusion **30** (1990) 997.

[16] S. P. Hirshman and J. C. Whitson, Phys. Fluids **26** (1983) 3553.

[17] R. H. Fowler, et al., Phys. Fluids **28** (1985) 338.

[18] A. H. Boozer and G. Kuo-Petravic, Phys. Fluids **24** (1981) 851.

[19] T. H. Stix, Nucl. Fusion 15 (1975) 737.

[20] I. B. Bernstein and D. C. Baxter, Phys. Fluids **24** (1981) 108.

[21] G. D. Kerbel and M. G. McCoy, Phys. Fluids **28** (1985) 3629.

[22] A. A. Galeev, and R. Z. Sagdeev, Review of Plasma Physics, (LEONTOVICH, M.A., Ed.), Vol. 7, Consultants Bureau, New York, London, 257.

Table I. Main parameters of CHS and LHD

	CHS	LHD
number of helical coil l	2	2
number of field period m	8	10
number of pairs of poloidal field coils	4	3
major radius R [m]	1.0	3.9
minor radius a [m]	~ 0.20	~ 0.56
pitch modulation parameter of winding law α	0.3	0.1
shift of magnetic axis Δ [m](standard)	-0.08	-0.15
strength of central magnetic field B_0 [T]	~ 2.0	3.0

Figure captions

FIG. 1. Mod-B_{min} contours of the the CHS plasma in the Boozer coordinates with two different major radius; (a) R = 0.888m and (b) R = 0.921m.

FIG. 2. Plots of the transfer power to the bulk plasma, P_{trans}, versus the absorption power by minority ions, P_{abs}, in the CHS plasma with R = 0.888m. The closed circles, squares, and triangles show the simulation results of B = 2.0T, 1.4T, and 0.92T, respectively.

FIG. 3. Plots of the heating efficiency, η, versus the absorption power by minority ions, P_{abs}, in the CHS plasma. (a) Closed circles, squares, and triangles show the results of B = 2.0T, 1.4T, and 0.92T in the R = 0.888m case, respectively. (b) Open circles, squares, and triangles show the results of B = 2.0T, 1.4T, and 0.92T in the R = 0.921m case, respectively. The solid, doted, and dashed curves show the fitting curves given by $\eta = 1/(1 + P_{abs}/P_0)$.

FIG. 4. Plots of P_0 as a function of magnetic field strength, B in the two configurations; R = 0.888m (closed circles) and R = 0.921m (open circles). The curves show the relation $P_0 = \alpha B^{\gamma}$.

FIG. 5. Typical orbits of minority ions during the ICRF heating in the two configuration and two magnetic field strengths of CHS; (a) R = 0.888m and B = 2.0T, (b) R = 0.921m and B = 2.0T, and (c) R = 0.888m and B = 0.92T, where the initial velocities and positions are all same.

FIG. 6. Plots of the heating efficiency, η, versus the absorption power by minority ions, P_{abs}, in the LHD plasma. The solid line shows the fitting curve given by $\eta = 1/(1 + P_{abs}/P_0)$.

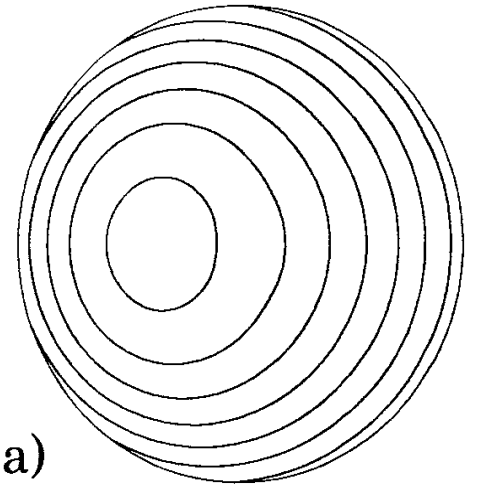

(a)

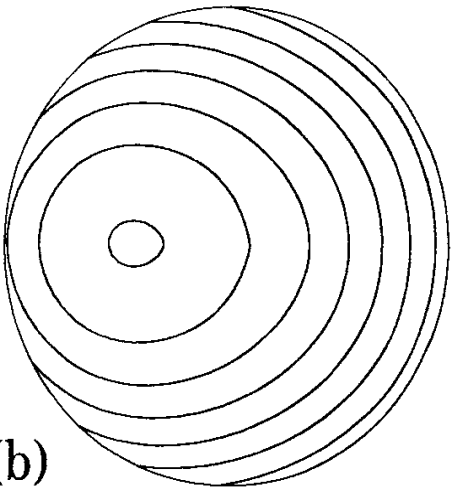

(b)

Fig. 1

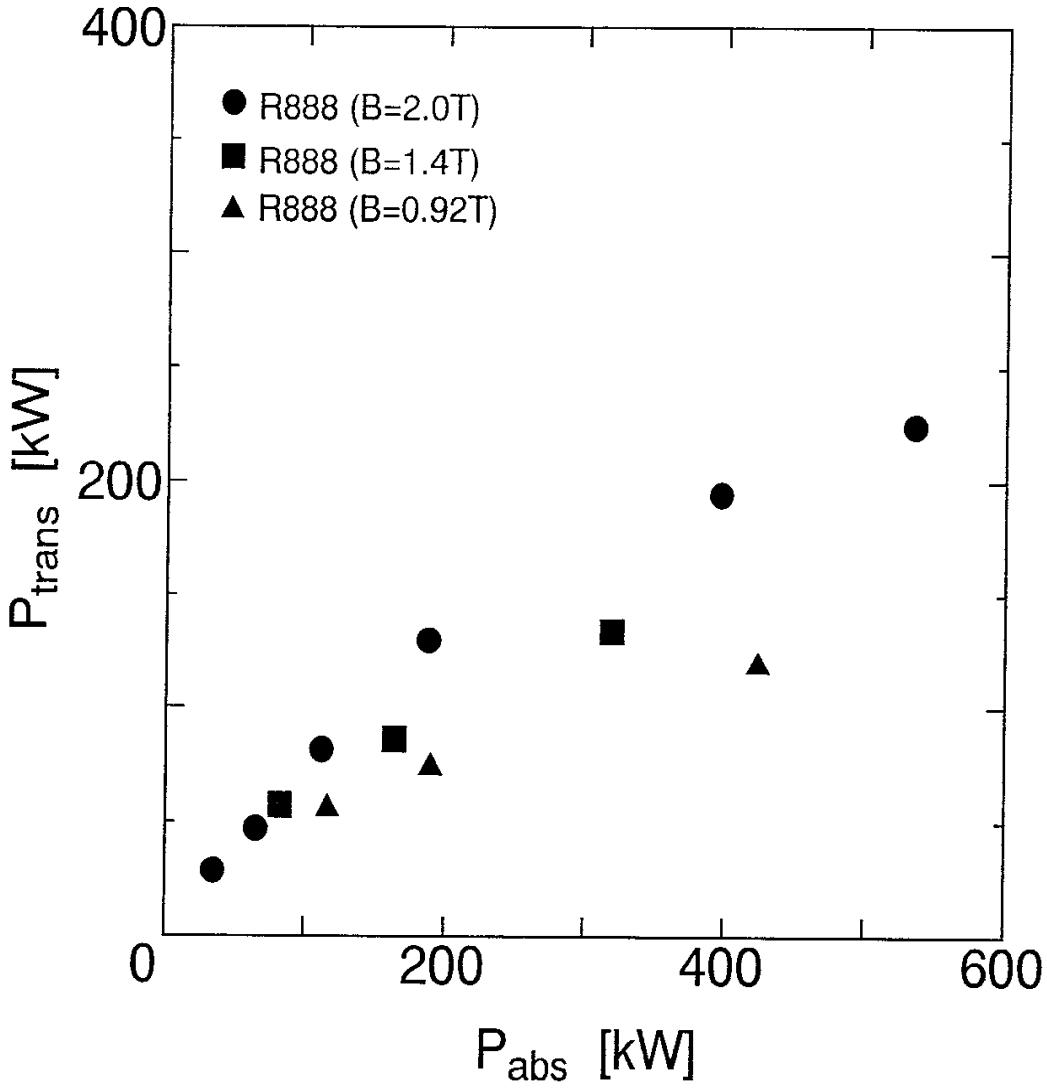
400
200
0
200
400
600
R888 (B=2.0T)
R888 (B=1.4T)
R888 (B=0.92T)
P trans [kW]
P abs [kW]

Fig. 2

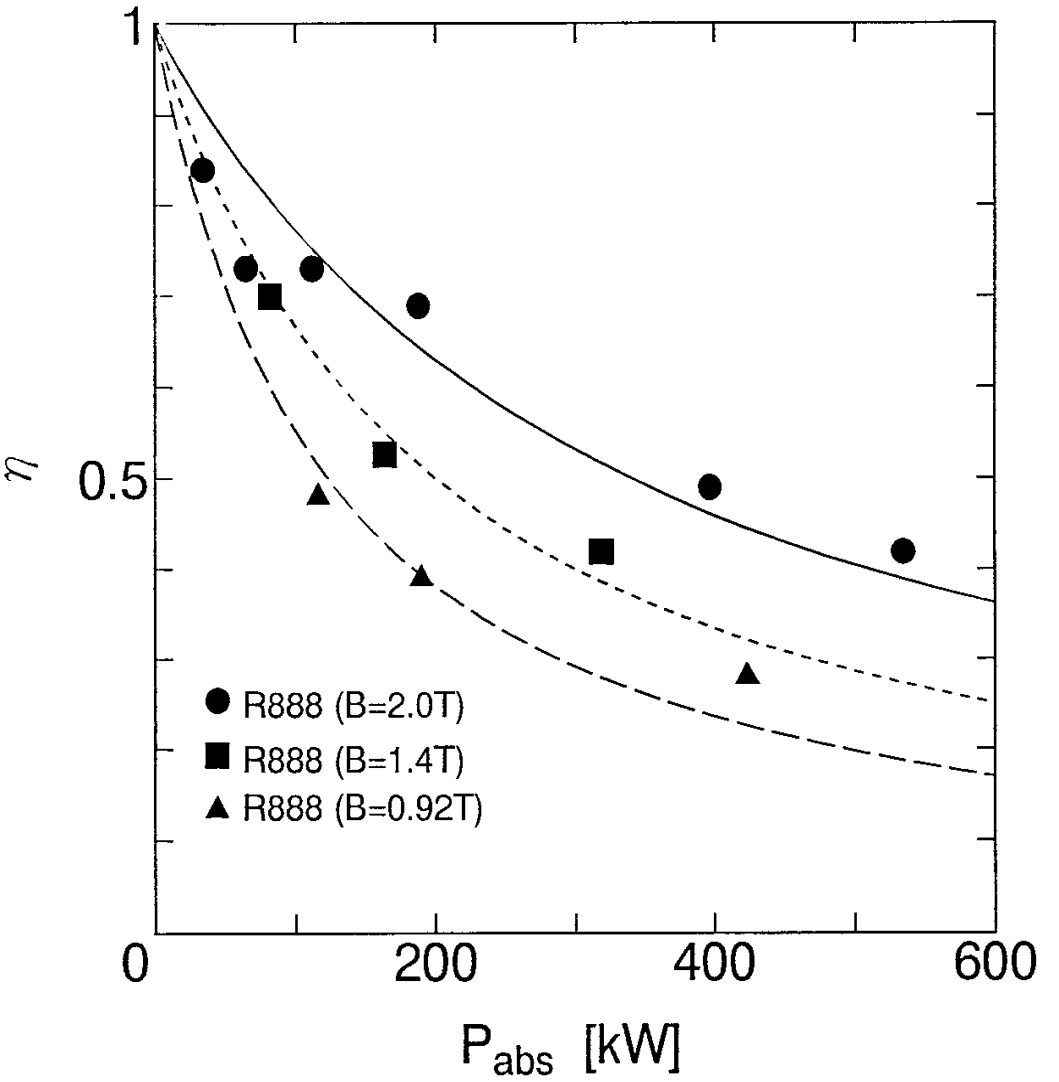

Fig. 3-(a)

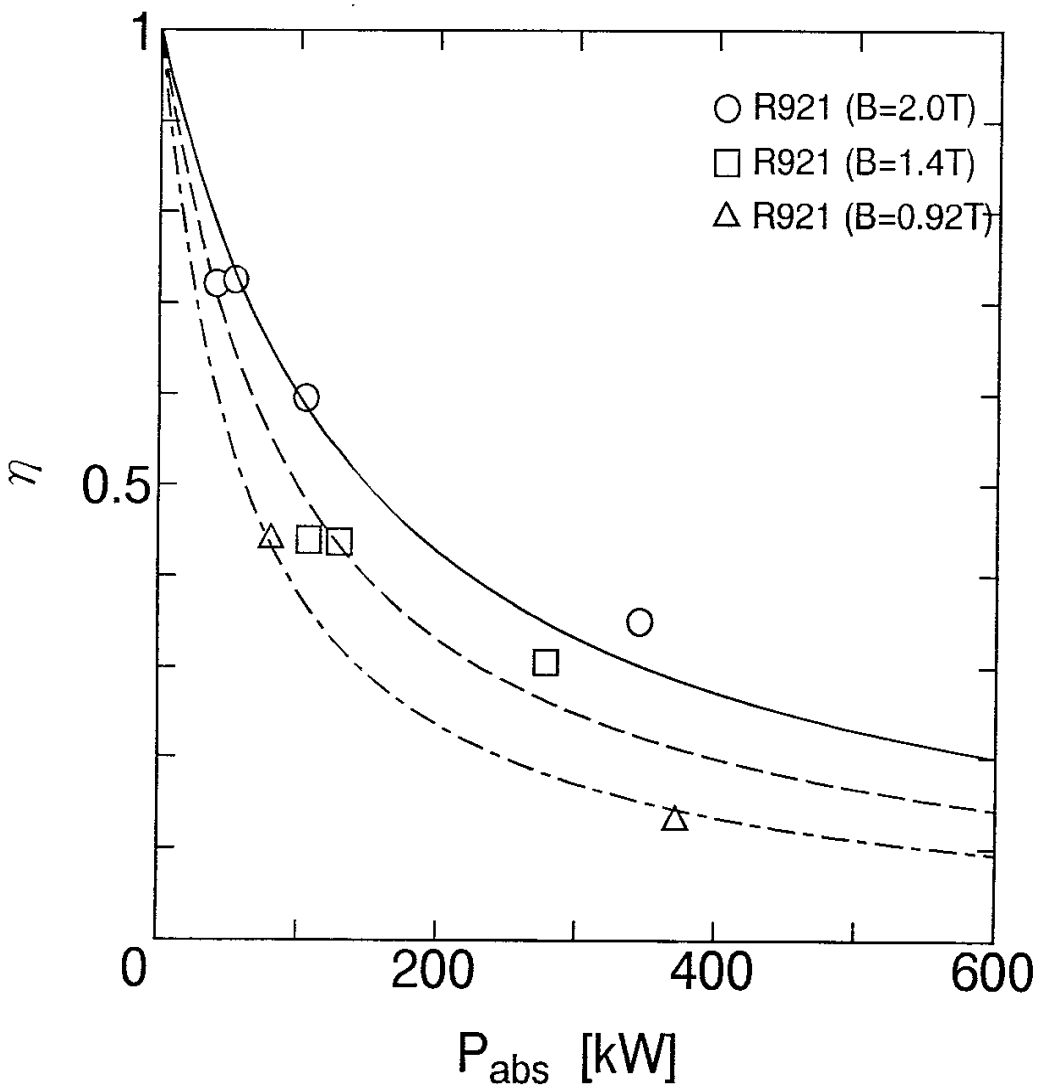

Fig. 3-(b)

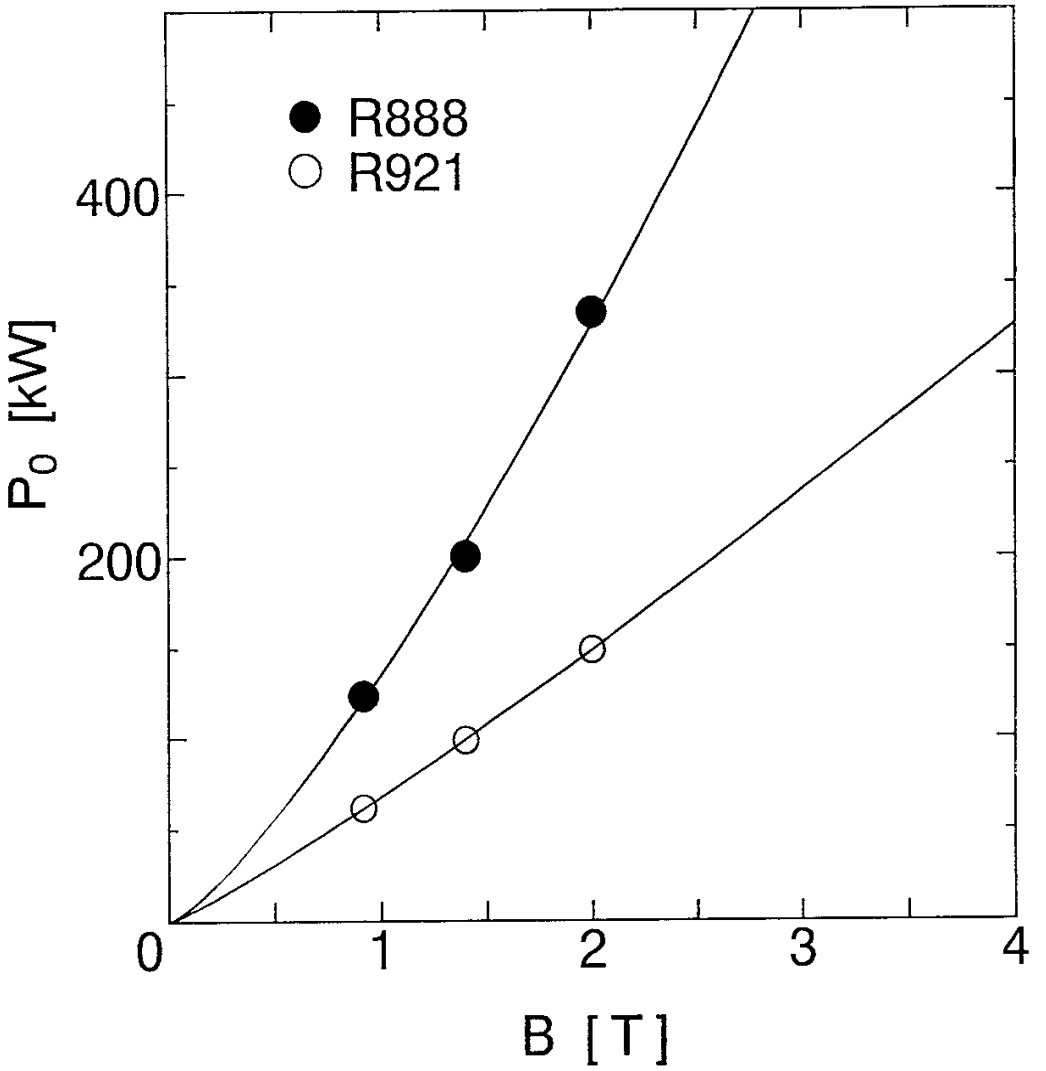

Fig. 4

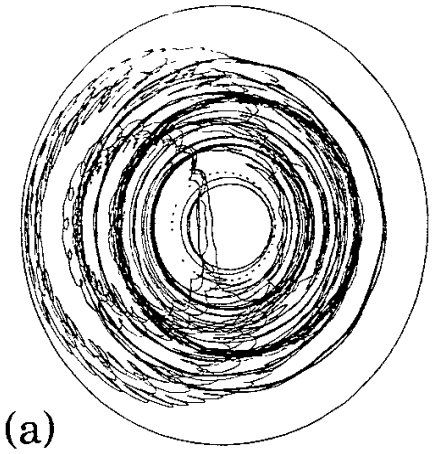

(a)

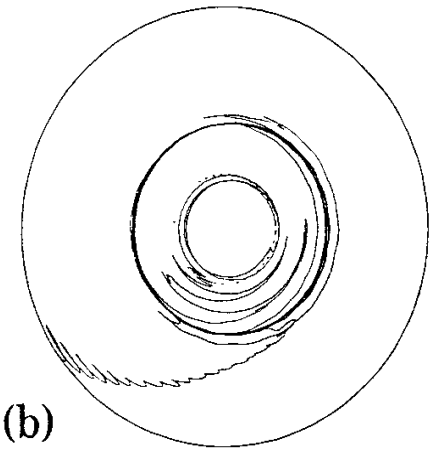

(b)

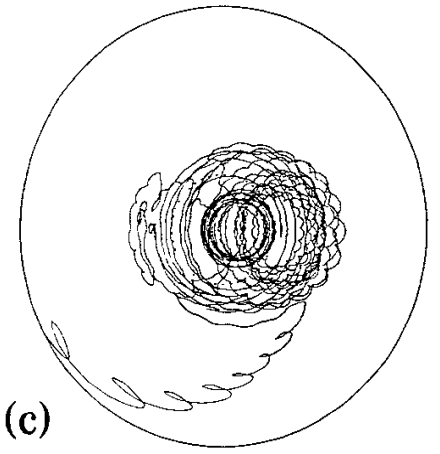

(c)

Fig. 5

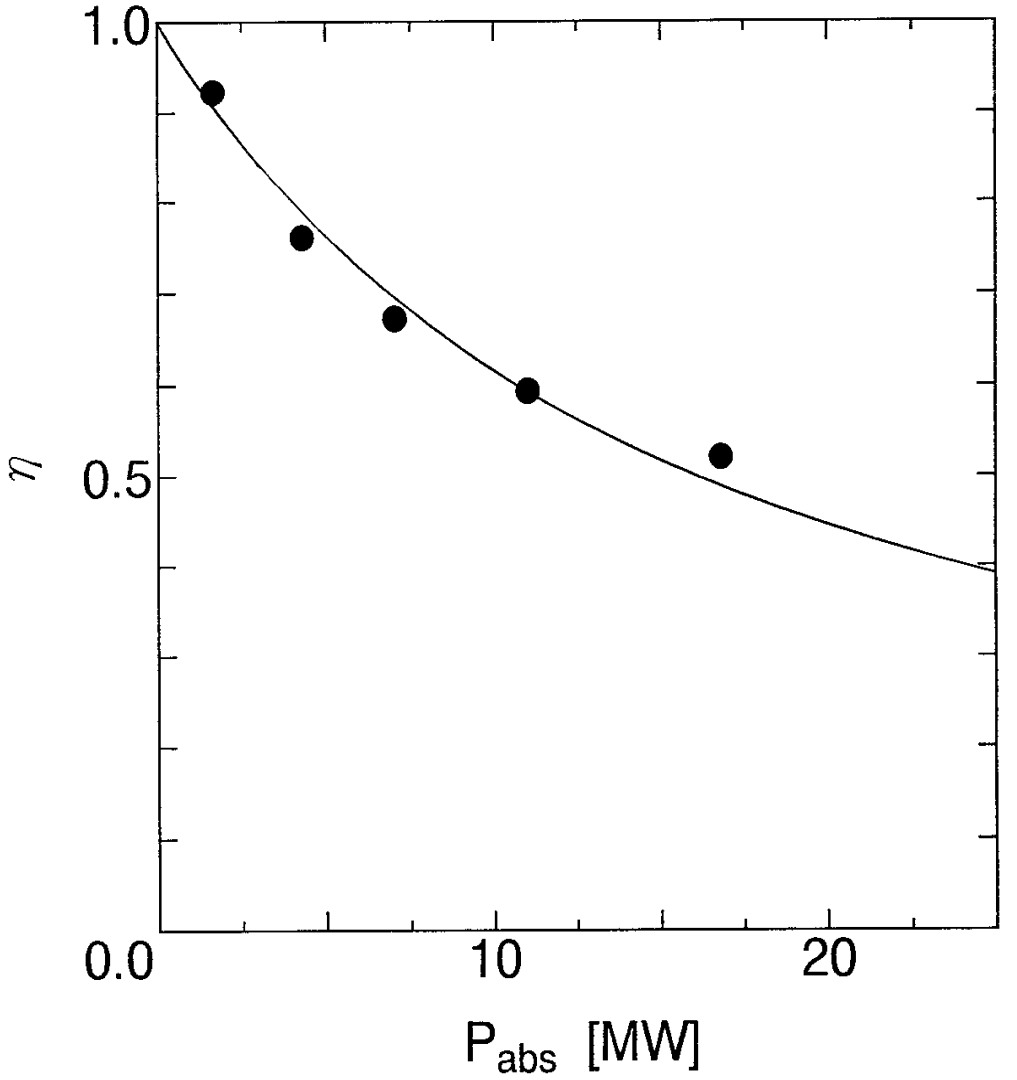

Fig. 6

Recent Issues of NIFS Series

NIFS-221 S.-I. Itoh, K. Itoh, and A. Fukuyama, *ELMy-H mode as Limit Cycle and Transient Responses of H-modes in Tokamaks* ; May 1993

NIFS-222 H. Hojo, M. Inutake, M. Ichimura, R. Katsumata and T. Watanabe, *Interchange Stability Criteria for Anisotropic Central-Cell Plasmas in the Tandem Mirror GAMMA 10 ;* May 1993

NIFS-223 K. Itoh, S.-I. Itoh, M. Yagi, A. Fukuyama and M. Azumi, *Theory of Pseudo-Classical Confinement and Transmutation to L-Mode;* May 1993

NIFS-224 M. Tanaka, *HIDENEK: An Implicit Particle Simulation of Kinetic-MHD Phenomena in Three-Dimensional Plasmas;* May 1993

NIFS-225 H. Hojo and T. Hatori, *Bounce Resonance Heating and Transport in a Magnetic Mirror;* May 1993

NIFS-226 S.-I. Iton, K. Itoh, A. Fukuyama, M. Yagi, *Theory of Anomalous Transport in H-Mode Plasmas;* May 1993

NIFS-227 T. Yamagishi, *Anomalous Cross Field Flux in CHS ;* May 1993

NIFS-228 Y. Ohkouchi, S. Sasaki, S. Takamura, T. Kato, *Effective Emission and Ionization Rate Coefficients of Atomic Carbons in Plasmas;* June 1993

NIFS-229 K. Itoh, M. Yagi, A. Fukuyama, S.-I. Itoh and M. Azumi, *Comment on 'A Mean Field Ohm's Law for Collisionless Plasmas;* June 1993

NIFS-230 H. Idei, K. Ida, H. Sanuki, H. Yamada, H. Iguchi, S. Kubo, R. Akiyama, H. Arimoto, M. Fujiwara, M. Hosokawa, K. Matsuoka, S. Morita, K. Nishimura, K. Ohkubo, S. Okamura, S. Sakakibara, C. Takahashi, Y. Takita, K. Tsumori and I. Yamada, *Transition of Radial Electric Field by Electron Cyclotron Heating in Stellarator Plasmas;* June 1993

NIFS-231 H.J. Gardner and K. Ichiguchi, *Free-Boundary Equilibrium Studies for the Large Helical Device,* June 1993

NIFS-232 K. Itoh, S.-I. Itoh, A. Fukuyama, H. Sanuki and M. Yagi, *Confinement Improvement in H-Mode-Like Plasmas in Helical Systems,* June 1993

NIFS-233 R. Horiuchi and T. Sato, *Collisionless Driven Magnetic Reconnection,* June 1993

NIFS-234 K. Itoh, S.-I. Itoh, A. Fukuyama, M. Yagi and M. *Azumi, Prandtl*

Number of Toroidal Plasmas; June 1993

NIFS-235 S. Kawata, S. Kato and S. Kiyokawa , *Screening Constants for Plasma;* June 1993

NIFS-236 A. Fujisawa and Y. Hamada, *Theoretical Study of Cylindrical Energy Analyzers for MeV Range Heavy Ion Beam Probes;* July 1993

NIFS-237 N. Ohyabu, A. Sagara, T. Ono, T. Kawamura and O. Motojima, *Carbon Sheet Pumping;* July 1993

NIFS-238 K. Watanabe, T. Sato and Y. Nakayama, *Q-profile Flattening due to Nonlinear Development of Resistive Kink Mode and Ensuing Fast Crash in Sawtooth Oscillations;* July 1993

NIFS-239 N. Ohyabu, T. Watanabe, Hantao Ji, H. Akao, T. Ono, T. Kawamura, K. Yamazaki, K. Akaishi, N. Inoue, A. Komori, Y. Kubota, N. Noda, A. Sagara, H. Suzuki, O. Motojima, M. Fujiwara, A. Iiyoshi, *LHD Helical Divertor;* July 1993

NIFS-240 Y. Miura, F. Okano, N. Suzuki, M. Mori, K. Hoshino, H. Maeda, T. Takizuka, JFT-2M Group, K. Itoh and S.-I. Itoh, *Ion Heat Pulse after Sawtooth Crash in the JFT-2M Tokamak;* Aug. 1993

NIFS-241 K. Ida, Y.Miura, T. Matsuda, K. Itoh and JFT-2M Group, *Observation of non Diffusive Term of Toroidal Momentum Transport in the JFT-2M Tokamak;* Aug. 1993

NIFS-242 O.J.W.F. Kardaun, S.-I. Itoh, K. Itoh and J.W.P.F. Kardaun, *Discriminant Analysis to Predict the Occurrence of ELMS in H-Mode Discharges;* Aug. 1993

NIFS-243 K. Itoh, S.-I. Itoh, A. Fukuyama, *Modelling of Transport Phenomena;* Sep. 1993

NIFS-244 J. Todoroki, *Averaged Resistive MHD Equations;* Sep. 1993

NIFS-245 M. Tanaka, *The Origin of Collisionless Dissipation in Magnetic Reconnection;* Sep. 1993

NIFS-246 M. Yagi, K. Itoh, S.-I. Itoh, A. Fukuyama and M. Azumi, *Current Diffusive Ballooning Mode in Seecond Stability Region of Tokamaks;* Sep. 1993

NIFS-247 T. Yamagishi, *Trapped Electron Instabilities due to Electron Temperature Gradient and Anomalous Transport;* Oct. 1993

NIFS-248 Y. Kondoh,
Attractors of Dissipative Structure in Three Disspative Fluids; Oct. 1993

NIFS-249 S. Murakami, M. Okamoto, N. Nakajima, M. Ohnishi, H. Okada,
Monte Carlo Simulation Study of the ICRF Minority Heating in the Large Helical Device; Oct. 1993

NIFS-250 A. Iiyoshi, H. Momota, O. Motojima, M. Okamoto, S. Sudo, Y. Tomita, S. Yamaguchi, M. Ohnishi, M. Onozuka, C. Uenosono,
Innovative Energy Production in Fusion Reactors; Oct. 1993

NIFS-251 H. Momota, O. Motojima, M. Okamoto, S. Sudo, Y. Tomita, S. Yamaguchi, A. Iiyoshi, M. Onozuka, M. Ohnishi, C. Uenosono,
Characteristics of D-^{3}He Fueled FRC Reactor: ARTEMIS-L, Nov. 1993

NIFS-252 Y. Tomita, L.Y. Shu, H. Momota,
Direct Energy Conversion System for D-^{3}He Fusion, Nov. 1993

NIFS-253 S. Sudo, Y. Tomita, S. Yamaguchi, A. Iiyoshi, H. Momota, O. Motojima, M. Okamoto, M. Ohnishi, M. Onozuka, C. Uenosono,
Hydrogen Production in Fusion Reactors, Nov. 1993

NIFS-254 S. Yamaguchi, A. Iiyoshi, O. Motojima, M. Okamoto, S. Sudo, M. Ohnishi, M. Onozuka, C. Uenosono,
Direct Energy Conversion of Radiation Energy in Fusion Reactor, Nov. 1993

NIFS-255 S. Sudo, M. Kanno, H. Kaneko, S. Saka, T. Shirai, T. Baba,
Proposed High Speed Pellet Injection System "HIPEL" for Large Helical Device
Nov. 1993

NIFS-256 S. Yamada, H. Chikaraishi, S. Tanahashi, T. Mito, K. Takahata, N. Yanagi, M. Sakamoto, A. Nishimura, O. Motojima, J. Yamamoto, Y. Yonenaga, R. Watanabe,
Improvement of a High Current DC Power Supply System for Testing the Large Scaled Superconducting Cables and Magnets; Nov. 1993

NIFS-257 S. Sasaki, Y. Uesugi, S. Takamura, H. Sanuki, K. Kadota,
Temporal Behavior of the Electron Density Profile During Limiter Biasing in the HYBTOK-II Tokamak; Nov. 1993

NIFS-258 K. Yamazaki, H. Kaneko, S. Yamaguchi, K.Y. Watanabe, Y.Taniguchi, O.Motojima, LHD Group,
Design of Central Control System for Large Helical Device (LHD); Nov. 1993

NIFS-259 K. Yamazaki, H. Kaneko, S. Yamaguchi, K.Y. Watanabe, Y.Taniguchi, O.Motojima, LHD Group,
Design of Central Control System for Large Helical Device (LHD); Nov. 1993

NIFS-260 B.V.Kuteev,
Pellet Ablation in Large Helical Device; Nov. 1993

NIFS-261 K. Yamazaki,
Proposal of "MODULAR HELIOTRON': Advanced Modular Helical System Compatible with Closed Helical Divertor; Nov. 1993

NIFS-262 V.D.Pustovitov,
Some Theoretical Problems of Magnetic Diagnostics in Tokamaks and Stellarators; Dec. 1993

NIFS-263 A. Fujisawa, H. Iguchi, Y. Hamada
A Study of Non-Ideal Focus Properties of 30° Parallel Plate Energy Analyzers; Dec. 1993

NIFS-264 K. Masai,
Nonequilibria in Thermal Emission from Supernova Remnants; Dec. 1993

NIFS-265 K. Masai, K. Nomoto,
X-Ray Enhancement of SN 1987A Due to Interaction with its Ring-like Nebula; Dec. 1993

NIFS-266 J. Uramoto
A Research of Possibility for Negative Muon Production by a Low Energy Electron Beam Accompanying Ion Beam; Dec. 1993

NIFS-267 H. Iguchi, K. Ida, H. Yamada, K. Itoh, S.-I. Itoh, K. Matsuoka, S. Okamura, H. Sanuki, I. Yamada, H. Takenaga, K. Uchino, K. Muraoka,
The Effect of Magnetic Field Configuration on Particle Pinch Velocity in Compact Helical System (CHS); Jan. 1993

NIFS-268 T. Shikama, C. Namba, M. Kosuda, Y. Maeda,
Development of High Time-Resolution Laser Flash Equipment for Thermal Diffusivity Measurements Usting Miniature-Size Specimens; Jan. 1994

NIFS-269 T. Hayashi, T. Sato, P. Merkel, J. Nührenberg, U. Schwenn,
Formation and 'Self-Healing' of Magnetic Islands in Finite-β Helias Equilibria; Jan. 1994